ISSN 1070-3284, Russian Journal of Coordination Chemistry, 2020, Vol. 46, No. 11, pp. 738–745. © Pleiades Publishing, Ltd., 2020.
Russian Text © The Author(s), 2020, published in Koordinatsionnaya Khimiya, 2020, Vol. 46, No. 11, pp. 663–671.

# Structure and Magnetic Properties of Superoxide Radical Anion Complexes with Low Binding Energy at the Graphene Edges

**V. Yu. Osipov[a, *], D. W. Boukhvalov[b, c], and K. Takai[d]**

[a] *Ioffe Institute, St. Petersburg, 194021 Russia*
[b] *Institute of Physics and Technology, Ural Federal University, Yekaterinburg, 620002 Russia*
[c] *College of Science, Institute of Materials Physics and Chemistry, Nanjing Forestry University, Nanjing, 210037 P.R. China*
[d] *Department of Chemical Science and Technology, Hosei University, Koganei, Tokyo, 184-8584 Japan*
**e-mail: osipov@mail.ioffe.ru*

Received April 19, 2020; revised May 6, 2020; accepted May 8, 2020

**Abstract**—The complexes of superoxide radical anions formed at the zigzag edges of curved graphene sheets upon microwave excitation were studied by electron spin resonance and quantum chemical density functional theory. The binding energy of the complex decreases from 700 to 42 meV as the distance between the oxygen atom and the zigzag graphene edge increases from 1.46 to 1.64 Å. The configurations and binding energies of the complexes depend both on the topology of the underlying graphene layer (single- or double-layer, flat, or curved) and on the type of atomic groups terminating the edge carbon atoms via σ-bonds. Complexes with low dissociation energy (<70 meV) can be formed only at cryogenic temperatures as a result of electronic charge transfer from the edge towards the $O_2$ molecule. The temperature behavior of the paramagnetic spin susceptibility of the complex indicates an antiferromagnetic interaction of the spin $S = 1/2$ of the $O_2^{-*}$ radical anions with the edge spins located outside the area "demagnetized" due to its depletion by the electronic charge. At $T > 50$ K, the complex irreversibly dissociates and the $O_2$ molecule is detached from the edge. The existence of complexes with a low dissociation energy expands the views on the ionic chemical bond with a large distance between the interacting species.

*Keywords:* superoxide radical anion, graphene, edge states, paramagnetic susceptibility, ESR spectroscopy
**DOI:** 10.1134/S107032842011007X

## INTRODUCTION

Graphenes and materials based on nanographene sheets are materials with extended π-electron system and unusual electronic properties [1–3]. These properties include both orbital diamagnetism [4–6], which substantially exceeds that observed for large planar aromatic molecules, and unusual paramagnetism caused by the edge electronic states at the zigzag edges [7–10]. The paramagnetism is related to the peak in the density of electron states at the contact point between graphene π- and π*-areas, while in terms of the Clar's aromatic sextet rule, it is associated with unpaired π-electrons located at every third zigzag along the zigzag edge [2, 11, 12] (Fig. 1). It is assumed that the external σ-bonds of the graphene sheets are saturated by functional groups: hydrogen and hydroxyl or carboxyl groups. The unusual π-electron states of the graphene edges account for their unusual chemical properties, in particular catalytic properties. The edges of specially perforated graphene efficiently catalyze the nitrobenzene reduction to aniline [13]. This is partly due to the fact that the edges act as π-electron donors for molecular agents occurring in the close vicinity and thus facilitate specific chemical reactions of these molecular agents.

Carbon nanomaterials, including fullerenes and multiwalled nanotubes, have been actively studied since the 1990s. In 1996, Mitsutaka Fujita, a Japanese Physicist, predicted the presence of unusual π-electron edge states for the zigzag edges of graphene sheets [14, 15]. Among the predicted unusual properties was paramagnetism caused by the unpaired edge spins. Over the next 15 years, edge states and Curie paramagnetism associated with them were noted for quite a few nanodispersed carbon materials with a high degree of graphitization in individual sheets and nanometer-scale fragments. These materials include nanographites, activated carbon fibers, turbostratic carbon, carbon nanohorns, graphene nanoflakes, and other $sp^2$-carbon products [16, 17]. The existence of edge states in flat graphene sheets was proved by scanning tunneling microscopy (STM) and scanning tunneling spectroscopy (STS) [18, 19]. The STM images demonstrate a clear-cut aromatic hexagonal structure as Clar's sextets with enhanced image brightness at the zigzag edges. Nevertheless, the edge π-electron spin

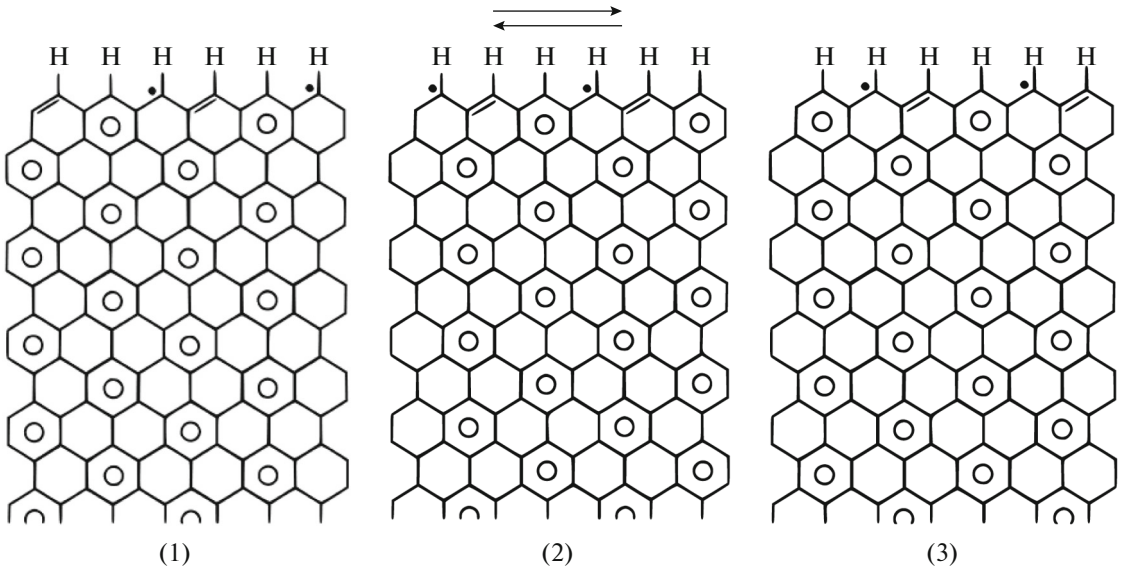


**Fig. 1.** Scheme of formation of delocalized spin states at the edges of a perfect graphene sheet representing the π-electron subsystem as Clar's aromatic π-sextets. Schemes (1), (2), and (3) are equivalent resonance configurations demonstrating the presence of delocalized spins at the zigzag edges (one spin per three aromatic rings).

states in combination with a relatively developed orbital diamagnetism and a high degree of graphitization of an $sp^2$-hybridized material are most clearly manifested in only one of the available materials, so-called nanographites obtained by annealing of detonation diamonds. It is known that orbital diamagnetism is a fundamental feature of a graphite material with a developed π-electron system, an aromatic layer structure, and the Fermi level located at the point of contact between the bonding π- and antibonding π*-bands. The text below is related to nanographites obtained from five-nanometer nanodiamonds. Nanographites obtained by this process represent a morphologically complex material, i.e., an assembly of onion-shaped carbon nanoparticles and associated split-off graphene-like parts of diverse topologies and shapes, including sub-nanometer ones. Therefore, in the discussion below, the elements of nanographite particles are designated for brevity as nanographenes. The π-electron states give rise to unusual paramagnetism and an ESR signal with the *g*-factor of 2.0014–2.0019 and line width highly sensitive to external molecular paramagnetic agents [20]. Indeed, in an oxygen (or air) atmosphere, the ESR line of the edge spins of nanographenes is considerably broadened due to the dipole–dipole and magnetic interactions with the triplet oxygen spins $S = 1$. Broadening depends on the amount of oxygen sorbed on the nanoparticles [21]. The maximum amount of oxygen sorbed from air at room temperature and normal pressure is ~55 $O_2$ molecules per nanoparticle (5–6 nm), consisting of ~11500 carbon atoms. ESR line broadening proportional to the partial pressure of oxygen is the criterion for the presence of localized edge states in the graphene-like carbon system.

Functionalization of the graphene zigzag edges by carbonyl groups leads to disappearance of the edge π-electrons and the peak in the density of electron states at the contact point between the π- and π*-bands, but the edge terminated in this way is readily additionally functionalized by $Fe^{2+}$ ions [22] (Scheme 1). For carbonyl groups of certain configurations, binding of iron(II) ions turns on again the π-electron edge states, and $Fe^{2+}$ ions can additionally bind molecular oxygen. These systems can act as catalysts and carriers of molecular oxygen released, for example, during microwave heating.

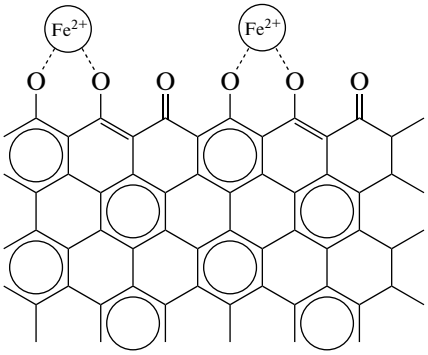


**Scheme 1.**

The images of nanographene/nanographite (NG) manufactured both by annealing of detonation diamonds and cleavage of acid-intercalated graphite into single- and multilayer graphene sheets were obtained using high-resolution transmission electron microscopy [13, 20, 23]. These images clearly demonstrate

the folds and curves of nanosized graphene sheets, areas of perfect hexagonal structure with good planarity, and particle edges.

This paper presents the results of studies performed by the authors in recent years on observation of the graphene edges of low-temperature complexes formed by superoxide radical anions connected to short-length zigzag edge segments (up to 7–8 zigzags) [24]. The formation of chemical bonds and complexes with low binding energies (<70 meV) at cryogenic temperatures has not been adequately studied and, therefore, deserves special attention. Graphene zigzag edge can also be considered as an element of a hypothetical planar aromatic molecule saturated with one type of atomic groups, e.g., atomic hydrogen, around the periphery with the number of hexagonal rings $N > 200$.

## EXPERIMENTAL

Polyhedral nanographite/nanographene with a particle size not more than 5–6 nm was prepared using commercially available detonation nanodiamond (DND) purified in boiling hydrochloric acid and free from ferromagnetic impurities. DND was annealed under argon at a temperature not lower than 1750°C for 35 and 110 min. The structural quality of nanographene particles was verified by Raman spectroscopy ($\lambda_{excit} = 532$ nm) by observing the characteristic G and D scattering bands at ~1590 and ~1345 $cm^{-1}$, associated with the basal graphene sheets and linear edge defects, respectively, and their 2D and D+G type overtones. The minimum content of pentagons and heptagons in aromatic hexagonal sheets was checked from the depth of the dip between the D- and G-bands, according to the methods described previously [23, 25]. The intrinsic magnetic properties of nanographite/nanographene were studied using powdered samples in evacuated sealed quartz tubes with an inner diameter of 0.8 mm and a length of not more than 45 mm, while the complexes of superoxide radical anions with graphene edges were studied using the same capillary tubes with the test material, but in this case, they were sealed in air at atmospheric pressure. The sample weight in the capillaries was not more than 0.8 mg. This weight limitation was dictated by the conductivity of the powdered sample and decrease in the resonator Q-factor in the case where the amount of the material was above the critical value (~1.4–1.6 mg). The two samples studied here were designated by ng35 and ng110. The extensions "air" or "vac" in the sample designations mean the type of atmosphere (air or vacuum) in the capillary at room temperature. The ESR spectra were recorded on an X-band EPR JEOL JES-FA 300 spectrometer (Japan) at a ~9.03 GHz microwave frequency. The sample was cooled using an Oxford Instrument ESR900 flow cryostat. The temperature was stabilized to an accuracy of at least ±0.03 K in the 3–100 K range and an accuracy of ±0.1 K in the 120–220 K range. For the ng35-air sample, pressure inside the capillary was lowered to below 20 Torr at $T < 60$ K due to sorption of the major gas components ($N_2$ and $O_2$), accompanied by liquefaction and solidification of molecular clusters on the nanoparticles and between them. The ESR signal intensities were corrected taking into account a small change in the resonator Q-factor with decreasing temperature and with the necessary increase in the sample weight for increasing the signal amplitude and signal-to-noise ratio. The change in the Q-factor was detected by the change in the intensity of specific ESR signals of the $Mn^{2+}$ : MgO standard. The intensities of the corrected ESR signals were directly proportional to the sample weights.

## RESULTS AND DISCUSSION

Figure 2 shows the temperature dependence of the integrated intensity of the ESR signal for NG-nanographene particles in the 5–300 K temperature range in a vacuum. Results of this type were first obtained in [21]. The paramagnetic spin susceptibility, which corresponds to the integrated intensity of the ESR signal, consists of two parts: the temperature-independent Pauli susceptibility ($\chi_P$) and the Curie component ($\chi_C$) related to the spins located at the zigzag edges; $\chi_C = C/(T - \Theta)$, where $C$ is the Curie constant proportional to the concentration of spins, $\Theta$ is the Weiss temperature, which is approximately −17 K for the nanographenes ng110 and is due to weak antiferromagnetic interaction of the edge spins with one another. The Pauli paramagnetism is associated with the π-electron subsystem of graphenes, and its magnitude is proportional to the local density of electron states at the Fermi level. Over a broad temperature range from 17 to 300 K, the spin susceptibility follows approximately the Curie law; when $T \approx 300$ K it depends on temperature only slightly and is mainly determined by the Pauli component: $\chi$ (300 K) ≈ $1.27\chi_P$. The ESR line width decreases with decreasing temperature in conformity with the Corringa law[1] (Fig. 2b): $\Delta H_{pp}(T)$ const + $(4\pi/\hbar) J^2_{edge-\pi} D(E_F)^2 k_B T$, here $\hbar$ is the Planck constant, $J_{edge-\pi}$ is the exchange integral for edge spins and π-electrons, $D(E_F)$ is the density of states at the Fermi level, $k_B$ is the Boltzmann constant, $T$ is temperature. The presence of this dependence is indicative of the presence of localized unpaired spins associated with exchange with charge carriers, i.e., π-electrons of the graphene sheet. The slope of the $\Delta H_{pp}(T)$ dependence in the 20–300 K range is dictated by the exchange integral $J_{edge-\pi}$ and by the density of states at the Fermi level. The arrow marks the inflection point in the $\Delta H_{pp}(T)$ plot, dividing the plot into

[1] Corringa law. In this experimental situation, this dependence is however nonlinear, and has a more complicated sublinear form at $T > 60$ K and a plateau at $T \leq 20$ K.

two segments with different trends along the temperature axis, quasi-linear one at $T = 20–55$ K and a sublinear one at $T > 60$ K (Fig. 2b). The latter may be attributable to the decrease in $D(E_F)$ or a change in the position of the Fermi level at temperatures above 60 K. With decreasing $T$, the edge unpaired π-electron is mainly localized near edges, namely, within a band with a width of 1 or 2 aromatic rings. At $T < 17$ K, the susceptibility slightly decreases (Fig. 2a). This is caused by antiferromagnetic interaction of some of the edge spins with molecular oxygen remaining on NG particles in trace amounts even after evacuation. This feature is eliminated on further sample evacuation with heating at ~673 K.

For the nanographene sample NG-air (ng35) sealed in a capillary with air,[2] lowering the temperature in the range from 293 to 145 K leads to broadening of the ESR signal of the edge π-electron states caused by the progressing sorption of paramagnetic oxygen on the basal planes and dipole–dipole mechanism of ESR line broadening (Fig. 3). At $T \approx 125$ K, the line is broadened to become almost non-observable, so that a narrow singlet with $g \approx 2.0024$ and the width $\Delta H_{pp} \approx 0.48$ mT, corresponding to defects such as dangling σ-bonds in the nanographene lattice or perhaps their oxygen complexes stable at room temperature, becomes visible against the background of this line[3] (Fig. 3, spectra at $T = 125–135$ K). Remarkably, this singlet is barely sensitive to the presence of triplet oxygen physisorbed on the material. On further lowering of the temperature to below 100 K, the broad signal is no longer detected, while the intensity of the narrow signal increases in the amplitude, but not quite according to the Curie–Weiss law (Fig. 3, spectra at $T = 73–93$ K). The width of the narrow signal does not depend on temperature and amounts to ~0.45 mT. In what follows, we analyze the temperature behavior of the narrow signal both during the gradual decrease in temperature down to 3–4 K and during the subsequent smooth heating of the capillary with the NG-air sample to 70–80 K after the formation of new paramagnetic complexes responsible for the generation of the "new" ESR signal with the same $g$-factor and line width, upon the microwave irradiation.

During thorough ESR studies of this system, we found unusual complexes formed by superoxide radical anion with the edge of the graphene sheet. These complexes were first experimentally observed in [26], while in [27], their formation was interpreted by quantum chemistry methods. The complexes appear when nanographenes located in a sealed capillary with air are cooled down to helium temperatures ($T \approx 5$ K) and

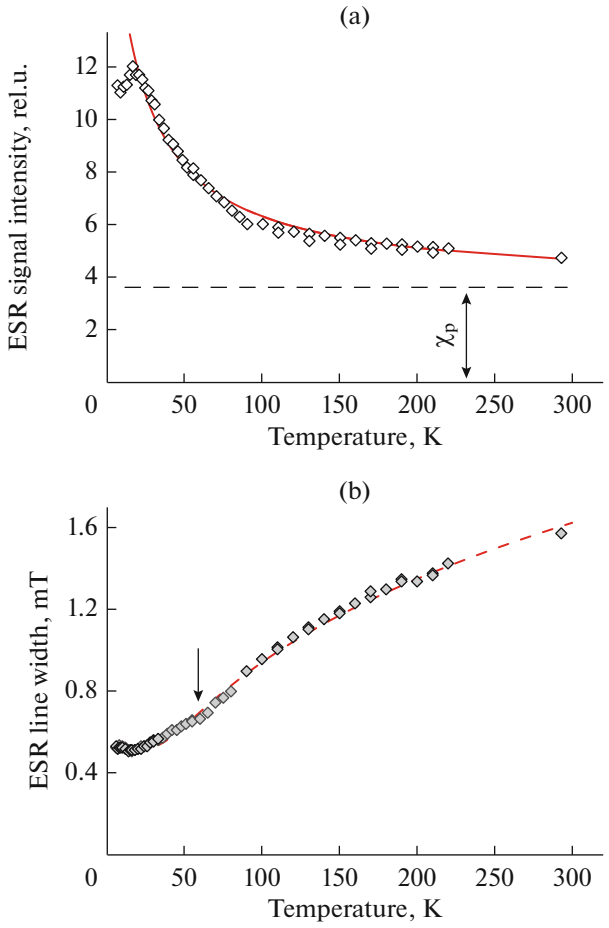


**Fig. 2.** Temperature dependence of the (a) integrated intensity and (b) width of the ESR signal for an evacuated nanographite sample ng110-vac linked to the edge π-electron states. Panel (a): dashed line is the temperature-independent Pauli component ($\chi_p$) of the paramagnetic susceptibility and continuous line is the Curie law smoothening ($\chi_c \approx (T-\Theta)^{-1}$) for the temperature-dependent component $\chi_c$. Pressure in the capillary: ~$2 \times 10^{-6}$ Torr. Microwave power: $P_{MW} = 0.02$ mW. Frequency: $\nu = 9.081$ GHz.

then the powder in the capillary is necessarily excited by microwave radiation with a power of up to 200 mW and an abrupt drop in the power to ~0.1 mW. The participation of oxygen in the formation of "new" paramagnetic centers is critical. According to [26], the complex is formed only in an oxygen-containing atmosphere upon electrostatic charging of powder nanoparticles and simultaneous heating by microwave eddy currents; during heating, the previously physisorbed molecular oxygen ($S = 1$) is first desorbed from the particle surface as a result of system overheating by 50–70 K and then is suddenly adsorbed again as the "heating" source is rapidly switched off. After the fast reverse sorption, some of the oxygen molecules are trapped at the edges to form new paramagnetic

[2] The electronic and magnetic properties of the nanographene powder in air (NG-air) differ appreciably from those for nanographene in a high vacuum (NG) due to adsorption of a large amount (up to 1.3 wt % or even more) of paramagnetic oxygen.

[3] The narrow signal is visible against the broad signal even at $T = 154$ K.

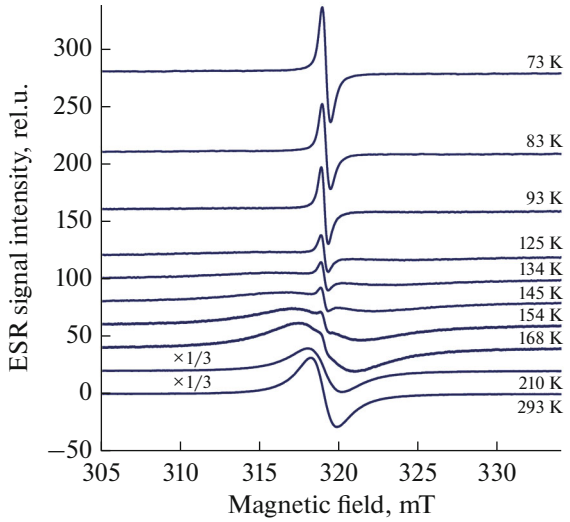


**Fig. 3.** Temperature dependence of the ESR signal for the nanographite sample ng35-air located in a sealed capillary in the air atmosphere (oxygen partial pressure ~150 Torr) measured during gradual temperature decrease from the room temperature to ~70 K (the curves show the temperature in Kelvins; microwave power: $P_{MW}$ = 0.1 mW; frequency ν = 8.941 GHz).

complexes, that is, ZE-$O_2^-$ dimers ($S_{ZE}$ = 1/2...S[$O_2^-$] = 1/2). Figure 4 shows the temperature dependence of the integrated intensity of the ESR signal of the NG-air sample measured in two modes: gradual lowering of the temperature from 290 to 5 K, with the spectra being recorded at low power $P_{MW}$ = 0.1 mW (curve *1*) and under microwave irradiation of the sample at $T$ = 5 K with the field of the cavity electromagnetic wave at the highest power ($P_{MW}$ = 200 mW) followed by power drop to the initial value $P_{MW}$ = 0.1 mW, with the spectra being recorded during gradual temperature rise to $T$ = 90 K (curve *2*). The difference between the integrated intensities (DIN) of signals *1* and *2* depending on the temperature describes the temperature behavior of the ESR signal corresponding to the low-temperature chemical complex, with the temperature of dissociation (destruction) of the complex being approximately 50 K. At temperatures above 50 K, the oxygen molecule is detached from the edge and the electron returns from $O_2^-$ to the zigzag edge (ZE). The complex is formed by the ionic bond upon the transfer of an electron from the edge (substrate) to an oxygen molecule that occurs near this edge. The ZE acts as the electron donor, while the oxygen molecule is the electron acceptor. Table 1 and Fig. 5 show the binding energies and some typical patterns of oxygen molecule fixing near the graphene edge calculated by the electron density functional theory for hydrogen- or hydroxyl- and carboxyl-terminated edges for sheets with different curvatures. The calculation details and the approximations used were described previously [27]. For the chosen complexes with the binding energy of up to 720 meV, the distances from the underlying graphene layer to the nearest oxygen atom ($d_{C-O}$) and the magnetic moments of $O_2^-$ were also calculated. As can be seen from Table 1, the lowest binding energies are inherent in ZE-$O_2^-$ complexes located near the curved surface of single- and/or double-layer graphene terminated by carboxyl groups and atomic hydrogen. The distance between the edge and one of the atoms of the oxygen molecule is longer (1.60–1.64 Å) than that for the same ZE-$O_2^-$ complex formed at a flat graphene sheet (1.46–1.50 Å), but shorter than that for the triplet oxygen molecule adsorbed on a flat graphene sheet via van der Waals forces (3.7 Å). Note that the ZE-$O_2^-$ complex is formed by the superoxide radical ion chemically bonded to the graphene edge. This bond is ionic for C–O distances of 1.60–1.64 Å and nearly covalent for distances of 1.46–1.53 Å. This is confirmed by comparison of the C–O distances with typical covalent C–O bond lengths (1.43 Å for most compounds and 1.54 Å for some molecules [28]). The electron transfer from the substrate to the oxygen molecule gives rise, as shown in [27], to a demagnetized[4] region shaped as a semicircle around the carbon site with the complex. Indeed, in the first row of carbon atoms along the zigzag, the magnetic moments in the lattice points are markedly reduced (by 0.25 $\mu_B$ for the central point forming the chemical bond and by 0.21, 0.15, and 0.1 $\mu_B$, respectively, for the first, second, and third points spaced apart from the first one by 2.4, 5.0, and 7.3 Å along the radius vector).

For the calculated ZE-$O_2^-$ complexes presented in Table 1, the binding energies were plotted versus the C–O distance and the magnetic moment of the $O_2^-$ ions (Figs. 6a, 6b). As the C–O distance increases from 1.46 to 1.64 Å and the $O_2^-$ magnetic moment increases from 0.86 to 0.965 $\mu_B$, the binding energy smoothly decreases from ~700 down to ~45 meV, in conformity with the trend of formation of low-temperature complexes with a low binduing energy and the spin $S$ = 1/2 of the $O_2^-$ component. The low binding energy of some of the complexes (<100 meV) and elongated C–O bond account for a moderately weak interaction between the ionic type agents, with only the van der Waals contact between the $O_2$ molecule and the flat graphene sheet being weaker than this contact. The binding energies, C–O distances, and $O_2^-$ magnetic moments corresponding to "conventionally low-temperature" complexes are encircled by dashed lines in Figs. 6a and 6b.

[4] This region is shaped as a semicircle, in each point of which the absolute magnetic moment of the carbon electron system is decreased by 1–25% relative to the total initial value.

The temperature dependence of the intensity of the ESR signal of the complex shown in Fig. 4 (curve *2*) can be described quite adequately in the $T < 55$ K range by the Bleaney–Bowers equation for complexes consisting of neighboring spins of 1/2, which are antiferromagnetically coupled and occur in the singlet ground state ($S = 0$) at zero $T$ in terms of the singlet–triplet model [29]. It is assumed here that the complex consists of two component spins of 1/2, one of which is the $O_2^{-*}$ radical anion spin and the other of which is the edge spin more remote from the first one along the edge. Since the amount of complexes sharply decreases at $T > 50$ K due to their dissociation or detachment of the superoxide radical anions from the edge, then DIN($T$) should be described using the product of the Bleaney–Bowers function and an empirical coefficient of filling of the edge adsorption sites by oxygen molecules ($S(T)$). The latter is a smoothened step function with broadening of about $\Delta T \approx 7$ K near $T_d \approx 47$–$50$ K: $S(T) = \left[\exp\left[(T - T_d)/\Delta T\right] + 1\right]^{-1}$, where $T_d$ is the effective desorption temperature of the $O_2^{-*}$ radical anions from the edge adsorption sites at which the molecule becomes neutral and quasi-free in two or three dimensions. In our case, $S(T)$ describes the relative number of chemically adsorbed agents on the surface of a solid in comparison with the number of specific adsorption sites that are completely filled in a particular sorption process, depending on the temperature. The singlet–triplet energy gap parameter found during fitting of the theoretical curve to experimental one is $2J/k_B \approx -22$ K.

Dissociation and degradation of the complex at temperatures above 50 K means that only few configurations with the curved graphene sheet, both single- and double-layer, and hydrogen- or carboxyl-terminated edge can provide for this behavior of the complexes. The binding energies for these four configurations are summarized in Table 1. The complexes with binding energies of ~70 meV are characterized by dissociation temperature of ~45 K, while for complexes with binding energy of 42–46 meV, these temperatures are at least 10 K lower. The estimates were referred to water vaporization energy, 0.46 eV/molecule at $T =$ 290 K and a pressure of ~15 Torr. Note that going from the multielectron to the single-electron model of the complex in terms of the electron density functional theory method is accompanied by a number of approximations and, hence, direct substitution of the calculated binding energies into thermodynamic relations becomes ill-posed. However, the temperature of dissociation can be estimated by indirect methods [30]. One of these methods is comparison of the binding energy calculated for the given case with the energy calculated for a system with known phase transition temperature and specific heat of vaporization of vaporization and with calculated intermolecular interaction energies. One of the systems with the modeled liquid–vapor transition is water. In this case, vaporization energy is spent for the destruction of collective hydrogen bonds between structural elements, that is, water molecules or clusters. The calculated averaged binding energy between two water molecules (~0.4 eV) coincides with the experimental specific heat of

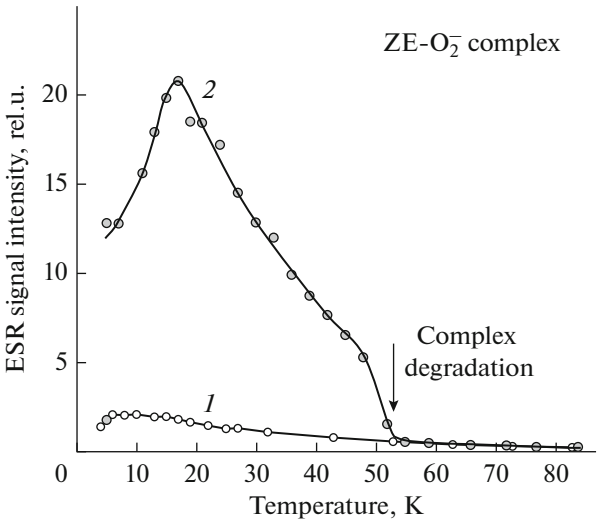


**Fig. 4.** Temperature dependences of the ESR signal of the ZE-$O_2^-$ complex in the nanographite sample ng35-air measured (curve *2*) after microwave irradiation at $T = 5$ K at 200 mW and (curve *1*) without irradiation. Curve *2* demonstrates the irreversible decomposition of complexes with a low binding energy (≤70 meV) at $T = 50$–$52$ K, $P_{MW} = 0.1$ mW. Frequency: ν = 8.941 GHz.

**Table 1.** Binding energies of ZE-$O_2^-$ calculated by electron density functional theory for graphene sheets with different edge thickness and type*

| Number of layers | Morphology | Binding energy, meV |
|---|---|---|
| 1 | Flat | 405[a] |
| | | 370[b] |
| | | 718[c] |
| | Curved | 72[a] |
| | | 68[b] |
| | | 478[c] |
| 2 | Flat | 160[a] |
| | | 142[b] |
| | | 208[c] |
| | Curved | 46[a] |
| | | 42[b] |
| | | 398[c] |

* Functional groups at the edge: [a] –H, [b] –COOH, [c] –OH.

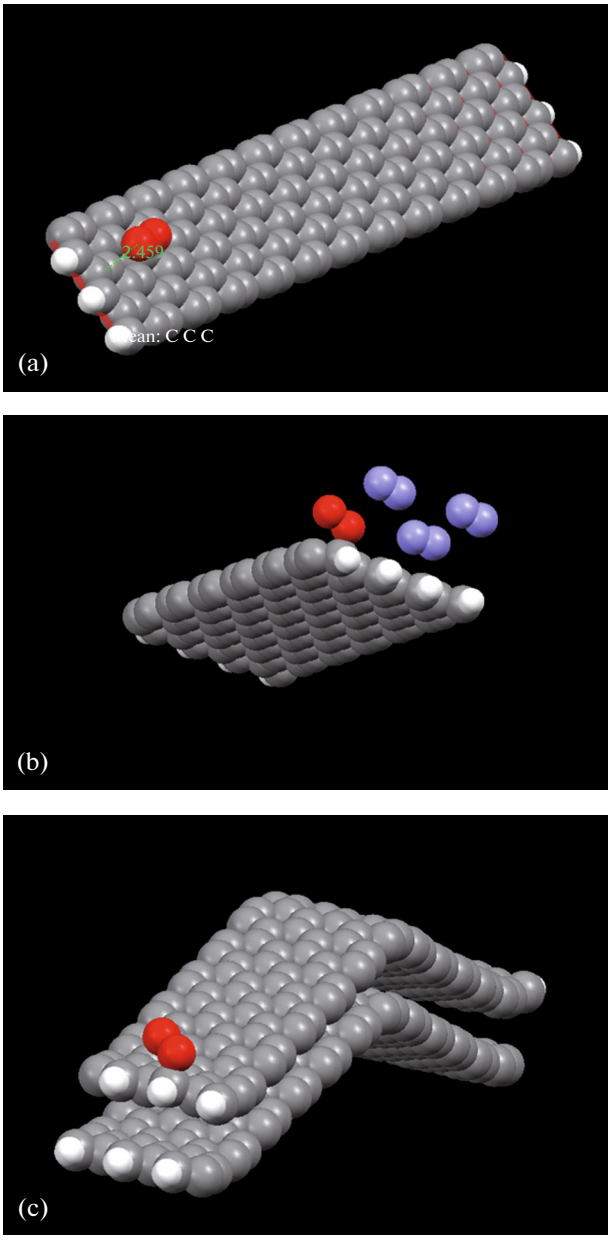


**Fig. 5.** Stereometric configurations calculated by electron density functional theory for (a) physisorbed $O_2$ molecule near the single-layer graphene edge (2.459 Å above the plane), (b) ZE-$O_2^-$ complex (binding energy: 1001 meV) and three nitrogen molecules physisorbed on the single-layer graphene edge, (c) ZE-$O_2^-$ complex with low dissociation energy (46 meV) on a curved two-layer graphene sheet. White color marks hydrogen atoms terminating the edge of the graphene sheet. The configurations were constructed using the Mercury program deposited at the Cambridge Crystallographic Data Centre (CCDC).

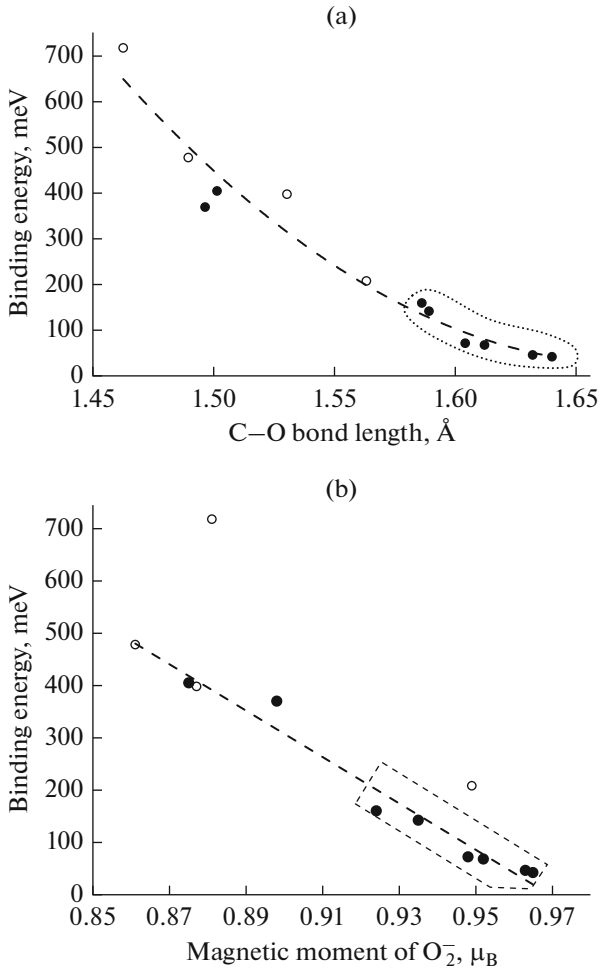


**Fig. 6.** DFT-calculated dependence of the binding energy of the ZE-$O_2^-$ complex formed at the graphene edge on the C–O bond length (a) and magnetic moment of the $O_2^-$ radical anion (b) for configurations with different ZE topology and types of functionalization of atomic groups. The dots encircled by a dashed line correspond to configurations of several complexes with binding energy of ≤160 meV (based on double- and single-layer curved graphene sheets with –H- and –COOH-functionalized edge).

vaporization to an accuracy of ~15%. Some details of this comparison are reported in [31, 32].

The oxygen molecule associated with the ZE edge of a flat single-layer graphene sheet has the highest binding energy in the range from 0.37 to 0.72 eV, irrespective of the type of surface functional groups (–H, –COOH, or –OH). For edges saturated only with OH groups, the binding energies are higher (~0.40–0.47 eV) even in the case of curved graphenes. These complexes are stable at room temperature and disappear only at $T > 373$ K or at higher temperatures (up to 500 K), e.g., simultaneously with the removal of sorbed water or other weakly bound adsorbates. Complexes with a low binding energy (≤72 meV) cannot appear at room temperature, while having appeared, e.g., under microwave or laser irradiation of the sample, they exist only at cryogenic temperatures ($T <$ 50 K). The difference of $O_2$ chemisorption on the edge from the physisorption on basal graphene planes is

that the chemisorption by the above mechanism is accompanied by transfer of an almost total electron charge (0.77–0.88 e) from the edge to the oxygen molecule. This changes the magnetic moments of both the oxygen molecule and at least three dozens graphene carbon atoms located under the oxygen molecule.

Thus, zigzag edge of the graphene sheet can form complexes with an oxygen molecule via π-electron transfer from the edge to oxygen. The complex formation and electron transfer from one component to the other take place at low temperature ($T \approx 5$ K) under microwave irradiation and electrostatic charging of some of the particles by eddy currents. The magnetic moments of components change when the complex is formed; the spin of the oxygen molecule decreases from 1 to 1/2 (due to the change in the charge state). A region of the graphene lattice located under the complex is "demagnetized." The dissociation energy of the complex depends on the curvature of the graphene sheet and on the number of graphene layers. The lowest binding energy (≤72 meV) is inherent in a curved graphene sheet with atomic hydrogen- or carboxyl-terminated edge. Planar graphene sheets form more stable complexes with oxygen with binding energy of ~0.37–0.72 eV. These complexes are stable at room temperature and can dissociate with the release of molecular oxygen in the range from ~400 to 500 K.

This effect may find application for trapping and storage of superoxide radical anions in nanographene powders at low temperatures for the subsequent controlled desorption of oxygen molecules.

## FUNDING

V. Yu. Osipov is grateful to the Japan Society for the Promotion of Science (JSPS) for the fellowship awarded to perform studies on this topic (JSPS Fellowship no. L17526). K. Takai is grateful to the JSPS KAKENHI for the support (projects 16K05758, 19K05410, 26107532).

## CONFLICT OF INTEREST

The authors declare that they have no conflicts of interest.

## REFERENCES

1. *Physics and Chemistry of Graphene: Graphene to Nanographene*, Enoki, T. and Ando, T., Eds., Singapore: Jenny Stanford, 2019, 2nd ed.
2. Zhang, J., Terrones, M., Park, C.R., et al., *Carbon*, 2016, vol. 98, p. 708.
3. Enoki, T., Takai, K., Osipov, V., et al., *Chem. Asian J.*, 2009, vol. 4, no. 6, p. 796.
4. McClure, J.W., *Phys. Rev.*, 1956, vol. 104, no. 3, p. 666.
5. Safran, S.A. and DiSalvo, F.J., *Phys. Rev. B*, 1979, vol. 20, p. 4889.
6. Panich, A.M., Osipov, V.Yu., and Takai, K., *New Carbon Mat.*, 2014, vol. 29, no. 5, p. 392.
7. Enoki, T. and Takai, K., *Solid State Commun.*, 2009, vol. 149, p. 1144.
8. Andersson, O.E., Prasad, B.L.V., Sato, H., et al., *Phys. Rev.*, 1998, vol. 58, p. 16387.
9. Osipov, V.Yu., Shames, A.I., Enoki, T., et al., *Diam. Relat. Mat.*, 2009, vol. 18, nos. 2–3, p. 220.
10. Wakabayashi, K., Fujita, M., Ajiki, H., and Sigrist, M., *Phys. Rev.*, 1999, vol. 59, p. 8271.
11. Solà, M., *Front Chem.*, 2013, vol. 1, p. A22.
12. Wassmann, T., Seitsonen, A.P., Saitta, A.M., et al., *J. Am. Chem. Soc.*, 2010, vol. 132, no. 10, p. 3440.
13. Savaram, K., Li, M., Tajima, K., et al., *Carbon*, 2018, vol. 139, p. 861.
14. Fujita, M., Wakabayashi, K., Nakada, K., and Kusakabe, K., *J. Phys. Soc. Jpn.*, 1996, vol. 65, p. 1920.
15. Nakada, K., Fujita, M., Dresselhaus, G., and Dresselhaus, M.S., *Phys. Rev.*, vol. 54, p. 17954.
16. Bandow, S., Kokai, F., Takahashi, K., et al., *Appl. Phys. A*, 2001, vol. 73, p. 281.
17. Takai, K., Oga, M., Sato, H., et al., *Phys. Rev. B*, 2003, vol. 67, p. 214202.
18. Kobayashi, Y., Fukui, K., Enoki, T., and Kusakabe, K., *Phys. Rev. B*, 2006, vol. 73, p. 125415.
19. Kobayashi, Y., Fukui, K., Enoki, T., et al., *Phys. Rev. B*, 2005, vol. 71, p. 193406.
20. Osipov, V.Yu., Enoki, T., Takai, K., et al., *Carbon*, 2006, vol. 44, p. 1225.
21. Osipov, V.Yu., Shames, A.I., Enoki, T., et al., *Diam. Relat. Mat.*, 2010, vol. 19, nos. 5–6, p. 492.
22. Panich, A.M., Shames, A.I., Tsindlekht, M.I., et al., *J. Phys. Chem. C*, 2016, vol. 120, p. 3042.
23. Bogdanov, K., Fedorov, A., Osipov, V., et al., *Carbon*, 2014, vol. 73, p. 78.
24. Enoki, T., Kobayashi, Y., Katsuyama, C., et al., *Diam. Relat. Mat.*, 2007, vol. 16, no. 12, p. 2029.
25. Osipov, V.Yu., Baranov, A.V., Ermakov, V.A., et al., *Diam. Relat. Mat.*, 2011, vol. 20, no. 2, p. 205.
26. Shames, A.I., Osipov, V.Yu., Vul', A.Ya., et al., *Carbon*, 2013, vol. 61, p. 173.
27. Boukhvalov, D.W., Osipov, V.Yu., Shames, A.I., et al., *Carbon*, 2016, vol. 107, p. 800.
28. Gunbas, G., Hafezi, N., Sheppard, W.L., et al., *Nature Chem.*, 2012, vol. 4, p. 1018.
29. Bleaney, B. and Bowers, K.D., *Proc. R. Soc. London. A*, 1952, vol. 214, p. 451.
30. Boukhvalov, D.W., Dreyer, D.R., Bielawski, C.W., and Son, Y.-W., *ChemCatChem*, 2012, vol. 4, no. 11, p. 1844.
31. Lee, C., Chen, H. and Fitzgerald, G., *J. Chem. Phys.*, 1995, vol. 102, p. 1266.
32. Reznikov, V.A., *Fazovye Perekhody, Mezhfaznye granitsy i nanotekhologii*, 2014, no. 4, p. 93. http://pti-nt.ru/ru/issue/publication/61-k-ponyatiyu-vodorodnoiy-svyazi-i-energii-svyazi-v-vode.

*Translated by Z. Svitanko*